Design of Lateral-Current-Injection-Type Membrane Distributed-Feedback Lasers for On-Chip Optical Interconnections

Takahiko Shindo, *Member, IEEE*, Mitsuaki Futami, Kyohei Doi, Tomohiro Amemiya, *Member, IEEE*, Nobuhiko Nishiyama, *Senior Member, IEEE*, and Shigehisa Arai, *Fellow, IEEE*

***Abstract*—For application to on-chip optical interconnections, lateral-current-injection (LCI) membrane distributed-feedback (DFB) lasers, which are expected to be potential components for such an application, were investigated from the aspects of low threshold current operation and high-speed direct modulation capability. First, the stripe width dependence of the carrier injection delay time was evaluated from small-signal response measurements of LCI Fabry–Perot lasers prepared on a semi-insulating InP substrate, and it was found that a narrower stripe width was advantageous for shorter carrier injection delay time as well as higher internal quantum efficiency. Second, semiconductor core layer thickness dependences of the lasing properties of LCI-membrane-DFB lasers, such as the threshold current, output power, relaxation oscillation frequency, and a 3-dB bandwidth, were investigated theoretically. A strong optical confinement effect in the semiconductor membrane structure enabled the design of an LCI-membrane-DFB laser with a low threshold current of 0.16 mA, an output power of more than 0.16 mW, and a high relaxation oscillation frequency of 8.9 GHz at a bias current of only 1 mA. From these values, the LCI-membrane-DFB laser can be a good candidate for a low-pulse-energy (<100 fJ/bit) light source, for high-speed (>10 Gb/s) transmission, and for on-chip optical interconnections.**

***Index Terms*—Distributed-feedback (DFB) laser, lateral current injection, membrane laser, optical interconnection, semiconductor laser.**

I. Introduction

OPTICAL fiber communication systems are being used not only in telecommunication links but also in short-distance high-speed networks such as local area networks (LANs) or data center networks. Furthermore, as a replacement for electrical wiring, optical interconnections are being studied extensively for board-to-board, chip-to-chip, and on-chip interconnections.

So far, progress in the processing speed and integration density of large-scale integrated (LSI) circuits has followed Moore's law. However, as scaling advances, this progress will soon confront limitations associated with resistor–capacitor (*RC*) delay or ohmic heating in the electrical interconnections [1], [2]. Optical interconnection is expected to be an alternative to solve this problem in future LSIs [3]–[5]. In optical devices for on-chip optical interconnection, low power dissipation and compactness carry significant weight compared with conventional optical devices. The available power consumption (energy cost for data transport) for signal sources such as a semiconductor laser in an on-chip optical interconnection is estimated to be 100 fJ/bit or less [6]. It simply means that the driving current of the light source is limited to less than 1 mA (with assumption of 10 Gb/s direct modulation and driving current of 1 V). Microcavity lasers such as vertical cavity surface-emitting lasers (VCSELs) [7]–[9] or microdisk lasers [10], [11] have been reported to be promising devices for ultralow threshold operation because of their strong optical confinement structures. Photonic crystal (PhC) lasers have also been extensively studied as low power consumption lasers [12], [13]. In particular, in recent years, electrically pumped PhC lasers have been demonstrated and have drawn considerable attention [14]–[16]. However, they have disadvantages such as low output or difficulty in controlling the output efficiency because optical confinement in an extremely small cavity is too strong.

Alternatively, we have proposed and demonstrated a semiconductor membrane laser that utilizes a high-index-contrast waveguide structure in the vertical direction. This membrane structure consists of a thin (several hundred nanometers) semiconductor core layer sandwiched between low-refractive-index cladding layers, such as air or SiO_2 instead of a semiconductor. Hence, the refractive-index difference between them reaches to approximately 40%, which is three to four times larger than that in conventional double-heterostructures (DHs), and the optical confinement factor into the active region (nowadays, quantum-well (QW) structures are often used) becomes about three times higher than that of the conventional DHs. Consequently, it also enhances a modal gain at the same injection carrier density, and leads to the realization of a low-threshold, short-cavity laser without sacrificing differential quantum efficiency. In our early works on membrane DFB lasers, very low-threshold continuous-wave (CW) operation with a stable single-mode property was confirmed under optical pumping [17]–[20]. So far, various structures for membrane lasers have been reported, such as a membrane laser bonded on a silicon-on-insulator (SOI) substrate [21] or a membrane laser with an airbridge structure

Manuscript received November 15, 2012; revised December 31, 2012; accepted January 21, 2013. Date of publication February 6, 2013; date of current version May 13, 2013.

T. Shindo, M. Futami, K. Doi, and N. Nishiyama are with the Department of Electrical and Electronic Engineering, Tokyo Institute of Technology, Tokyo 152-8552, Japan (e-mail: shindou.t.aa@m.titech.ac.jp; futami.m.aa@m.titech.ac.jp; doi.k.ac@m.titech.ac.jp; n-nishi@pe.titech.ac.jp).

T. Amemiya and S. Arai are with the Quantum Nanoelectronics Research Center, Tokyo Institute of Technology, Tokyo 152-8552, Japan (e-mail: amemiya.t.ab@m.titech.ac.jp; arai@pe.titech.ac.jp).

Color versions of one or more of the figures in this paper are available online at http://ieeexplore.ieee.org.

Digital Object Identifier 10.1109/JSTQE.2013.2244573

1077-260X/$31.00 © 2013 IEEE

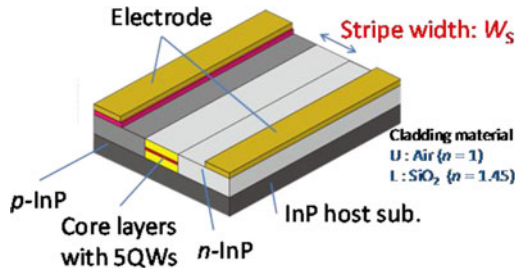

Fig. 1. Schematic diagram of an LCI-FP laser fabricated on the SI–InP substrate.

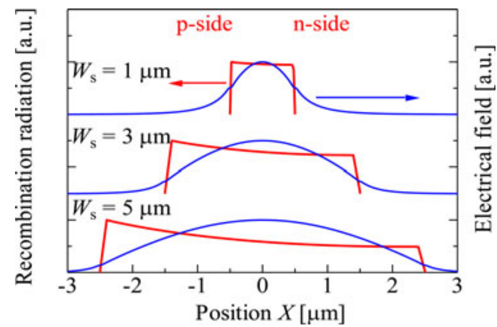

Fig. 2. Calculated distributions of carrier recombinations and optical mode profile determined from the equivalent index of the waveguide for different stripe widths.

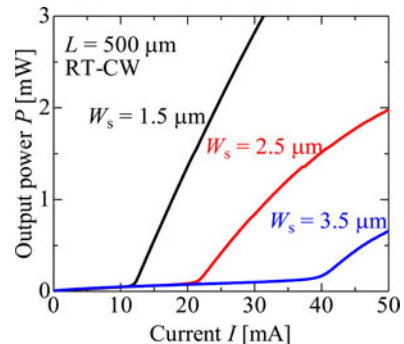

Fig. 3. Lasing characteristics of LCI-FP lasers with different stripe widths.

[22]. Furthermore, in order to realize electrical pumping of a membrane laser, we have investigated a lateral-current-injection (LCI) structure [23] formed by a two-step regrowth process. As a step to realize a current-injection-type membrane laser, up to now, high-performance LCI-type Fabry–Perot (FP) lasers [24], [25] and distributed-feedback (DFB) lasers [26], [27] on semi-insulating (SI) InP substrates have been demonstrated. Recently, electrically pumped DFB lasers with a surface grating structure have been also demonstrated by introducing an LCI structure [28], and a low threshold current of 3.8 mA was realized by using a benzocyclobutene (BCB) bonding process [29]. However, an ultralow threshold current operation was not achieved, because these devices had a relatively thick core layer of more than 450 nm and a certain error in the fabrication of the grating.

In this paper, the feasibility of the LCI-membrane-DFB laser as a light source for on-chip optical interconnection is theoretically examined from the aspects of low threshold current operation and high-speed direct modulation. In Section II, stripe width dependences on threshold current and carrier injection delay time of LCI lasers are described. Section III provides an explanation of the optical confinement factor of the active region in a membrane DFB laser, where enhancement of optical confinement in a high-index-contrast waveguide, equivalent refractive index, and index-coupling coefficient of the grating are described. Finally, Section IV discusses the dependences of threshold current and relaxation oscillation frequency on core layer thickness as well as the 3-dB bandwidth of an LCI-membrane-DFB laser.

II. Stripe Width Dependence of LCI-Type Lasers

The structure of an LCI laser is quite different from that of conventional laser diodes (LDs). In an LCI laser, electrons and holes are injected into the active region from n-InP and p-InP cladding layers placed on the sides of the active region stripe, as shown in Fig. 1. In this structure, carrier recombination tends to occur in eccentrically located regions near the p-InP side since the mobility of electrons is much higher than that of holes. Fig. 2 shows the calculated distribution of carrier recombination and the optical mode profile defined by the equivalent index of the waveguide for different stripe widths at current levels slightly below the threshold. In the LCI structure, carrier nonuniformity in the stripe arises which becomes apparent in wide stripe structures. However, the calculated optical mode profile of the fundamental mode, which is determined by the waveguide structure of the device, has a peak at the center of a stripe. This displacement of the carrier recombination profile from the optical mode profile suppresses carrier consumption coupled to the oscillation mode. However, in the case of a narrow stripe, this nonuniformity of the carrier recombination becomes less pronounced, and the modal gain at a fixed injected carrier density becomes larger, which leads to a lower threshold current density.

In order to confirm the aforementioned tendency, we fabricated LCI-type FP cavity lasers with various stripe widths (1.5, 2.5, and 3.5 μm) prepared on SI InP substrates, as shown in Fig. 1 and measured their threshold currents and differential quantum efficiencies. The total thickness grown on the SI–InP substrate was approximately 400 nm, and the active region consisted of compressively strained 5 quantum wells (5QWs) with 6-nm-thick wells and 9-nm-thick barriers sandwiched between 160-nm-thick GaInAsP optical confinement layers (OCLs), and a 10-nm undoped InP top layer. As a result, the narrower stripe devices showed not only lower threshold current but also higher differential quantum efficiency for a cavity length of 500 μm, as shown in Fig. 3.

We plotted the reciprocal of the differential quantum efficiency η_d as a function of the cavity length L for these three different stripe widths and estimated the internal quantum efficiency η_i and the internal loss $\alpha_{\rm WG}$ by linear extrapolation, as shown in Fig. 4. As can be seen, η_i is larger when the stripe width is narrower, whereas the waveguide loss $\alpha_{\rm WG}$, which can be obtained from the slope and η_i, was almost the same for the three stripe widths. This strong dependence of η_i on stripe width is because of the increase of number of carriers which did

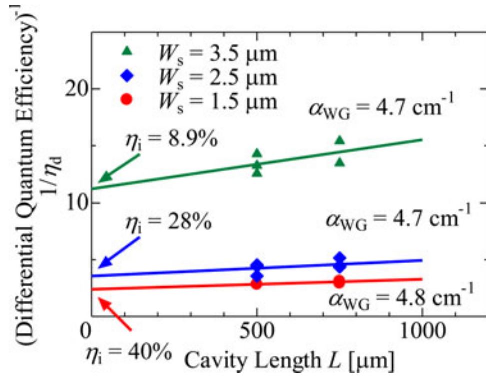

Fig. 4. Inverse of differential quantum efficiency of LCI-FP lasers fabricated on the SI–InP substrate as a function of cavity length.

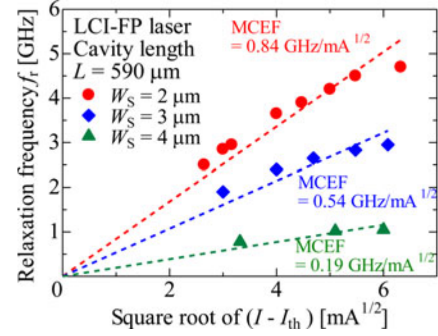

Fig. 5. Relaxation oscillation frequency of an LCI-FP laser as a function of (I–Ith)1/2 for various stripe widths.

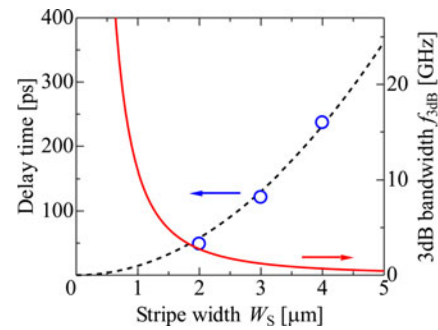

Fig. 6. Carrier injection delay time dependence on stripe width of LCI-FP lasers.

not contribute to the lasing operation due to nonuniform carrier profile. Even in the devices with the narrow width of 1.5 μm, η_i was suppressed up to 40%. We believe that this is due to nonradiative surface recombinations, probably between the top thin InP cover layer and air, and a larger fraction of injected carriers is captured in these nonradiative centers when the stripe width is wider. In fact, in order to suppress such nonradiative recombinations from the top thin InP cover layer, we separated the 5QWs by inserting GaInAsP layers so as to capture carriers into QWs efficiently and obtained η_i of approximately 70% [30], [31].

Unlike in the case of the internal quantum efficiency η_i, the waveguide loss α_{WG} had little dependence on the stripe width. However, there is a concern about the increase of α_{WG} of narrower stripe width due to an absorption loss increase in the p-InP clad region. Since the optical confinement factors in the p-InP clad region for the stripe widths of 3.5, 1.5, and 1.0 μm are calculated to be 0.2%, 1.5%, and 2.5%, respectively, α_{WG} of 1.0 μm stripe width is expected to be 4.9 cm^{-1}; therefore, we think it will not degrade the differential quantum efficiency even for the stripe width of 1.0 μm.

Next, the carrier injection delay time of LCI-type lasers was estimated by fitting to the small-signal response after bonding the devices onto an AlN coplanar submount for high-speed measurement by using the following formula:

$$M(f) = \frac{1}{1+(2\pi f\tau)^2} \cdot \frac{f_r^4}{(f^2 - f_r^2) + f^2\Gamma^2 \big/ (2\pi)^2} \quad (1)$$

where $M(f)$ is the modulation response for the frequency f, τ is the electrical delay time, f_r is the relaxation oscillation frequency, and Γ is the damping factor. Since the *RC* delay time is expected to be small compared with the carrier injection delay time in LCI-type lasers, the stripe width dependence of the small-signal response was observed for LCI-FP lasers with different stripe widths. The prepared devices were fabricated on the same wafer and had the same structure as that of a typical LCI-FP laser as reported in [25]. The cavity length of all these lasers was 590 μm, and their threshold currents were 10, 13, and 24 mA for stripe widths of 2, 3, and 4 μm, respectively.

Fig. 5 shows the relaxation oscillation frequency f_r of measured devices as a function of the square root of the bias current above the threshold $(I{-}I_{\mathrm{th}})^{1/2}$. In fact, these measured devices were different from the devices shown in Figs. 3 and 4, but they were fabricated from the same initial multiple quantum well (MQW) wafer using the same fabrication process. As can be seen, the modulation current efficiency factor (MCEF) was higher in narrower stripe devices, and the MCEF of a 2-μm-stripe device was 0.84 GHz/mA$^{1/2}$, which was almost four times higher than that (0.19 GHz/mA$^{1/2}$) of a 4-μm-stripe device. This large difference in the MCEF can be attributed to the low internal quantum efficiency of LCI-FP lasers with wide stripe widths as mentioned before.

Fig. 6 shows the estimated total delay time from small-signal modulation as a function of stripe width with a bias voltage of 1.5 V. As the stripe width became wider, the delay time monotonically increased. The estimated delay time can be considered to consist of three components, i.e., delay time due to carrier transit time in the OCL, carrier capture time from barrier layers to the QWs, and delay time due to the *RC* product of the LCI structure. Since carrier capture time is typically less than 1 ps [32], it does not affect the dynamics of our LCI lasers. Next, the delay time due to the *RC* product was also estimated to be less than 1 ps from an InP coplanar microstrip waveguide without a p–i–n junction, which has the same electrode structure as an LCI laser. Since the *RC* delay time is expected to be small compared with the carrier injection delay time in LCI-type lasers, the measured total delay time dependence on stripe width as shown in Fig. 6 can be governed mainly by carrier transit time in the OCLs. In the LCI structure, carrier transport distance corresponds to stripe width, which is much longer than

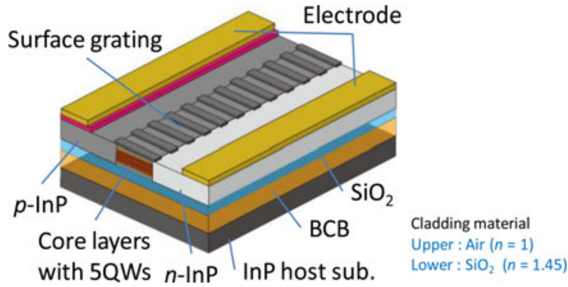

Fig. 7. Schematic diagram of an LCI-membrane-DFB laser with a surface grating structure.

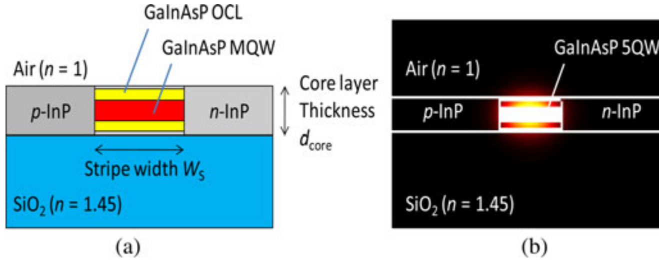

Fig. 8. Cross-sectional structure and optical mode field of an LCI-membrane laser. (a) Cross sectional structure. (b) Optical mode field.

that of a conventional semiconductor laser with a vertical current injection structure. The estimated delay time of a device with a stripe width of 2 μm is around 50 ps. In addition, the delay time with a stripe width of 1 μm is estimated to be around 15 ps. This is an adequate value for direct modulation at over 10 Gb/s.

III. Optical Confinement in Membrane Structure

As previously described, our ultimate target is the ultralow threshold current operation of an LCI membrane laser for on-chip optical interconnection. The optical confinement factor is one of the most important parameters for high-performance operation of a membrane laser. Therefore, the strong optical confinement effect of the membrane laser was theoretically investigated. Fig. 7 shows a schematic diagram of the LCI-membrane-DFB laser with a surface grating structure. The cross section of the device structure and a calculated optical mode field of the LCI-membrane laser are shown in Fig. 8. In this calculation, the upper and lower cladding materials are assumed to be air ($n = 1$) and SiO_2 ($n = 1.45$), respectively. In addition, p-InP and n-InP cladding layers are formed on both sides of the laser stripe. The number of the QWs is 5. This structure is the same as that of the LCI-membrane laser actually fabricated [28], [29].

Fig. 9 shows the core layer thickness dependence of the optical confinement factor in a single QW averaged over 5QWs, and that of the equivalent refractive index for the fundamental transverse mode, where the stripe width was assumed to be 1 μm. The cross-sectional layer structure used for this calculation is also indicated on the right-hand side of Fig. 9. In this calculation, the thicknesses of the active region (5QW) and InP cap layers were fixed at 90 and 10 nm, respectively, and only the OCL thickness was varied as a parameter. Therefore, the

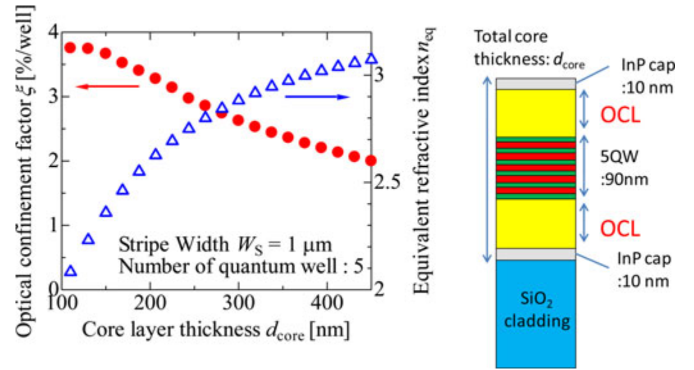

Fig. 9. Calculated optical confinement factor and equivalent refractive-index dependence on core layer thickness of an LCI-membrane laser.

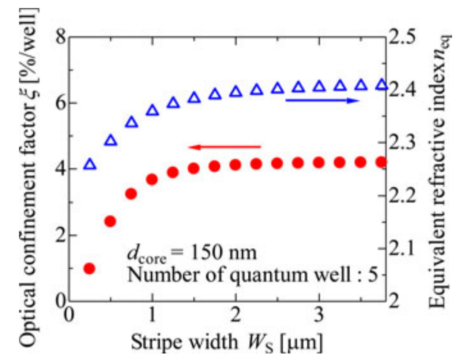

Fig. 10. Calculated optical confinement factor and equivalent refractive-index dependence on stripe width of an LCI-membrane laser.

minimum core layer thickness was 110 nm. As can be seen, the optical confinement factor can be enhanced by reducing the core layer thickness $d_{\rm core}$, and it reaches to 3.7%/well, which is almost three times higher than that of conventional semiconductor lasers, at $d_{\rm core} = 150$ nm. The optical confinement factor becomes nearly saturated when the core layer thickness is less than 150 nm. However, the equivalent refractive index decreases with the increase in the core layer thickness. The equivalent refractive index is estimated to be 2.60 at $d_{\rm core} = 150$ nm. In fact, the total thickness of GaInAsP OCLs is only 20 nm when the total core layer thickness is 150 nm; it is difficult to reduce the total core layer thickness to less than 150 nm without reducing the number of QWs.

Fig. 10 shows the dependences of the optical confinement factor and the equivalent refractive index on the stripe width of the LCI-membrane laser with $d_{\rm core} = 150$ nm. For low threshold current operation, a small active region volume, i.e., a narrow stripe, is preferable. Furthermore, high internal quantum efficiency and wide modulation bandwidth are also expected when a narrow stripe width is adopted as described in Section II. However, the optical confinement factor is reduced drastically when the stripe width is reduced to less than 1 μm. In the lateral direction of the LCI-membrane laser, the refractive-index difference between the core layer and the InP cladding layer is relatively small compared to that in the vertical direction. Therefore, it is difficult to realize a stripe width of less than 1 μm. As a solution,

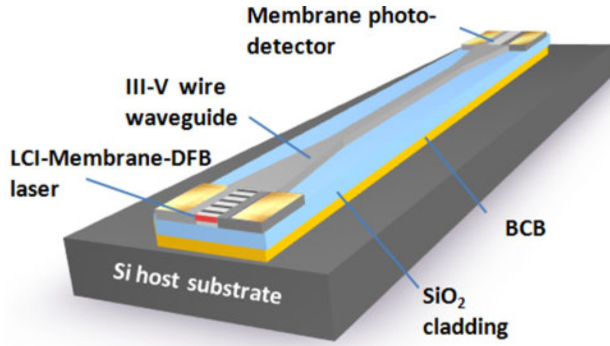

Fig. 11. Schematic diagram of a membrane-based PIC.

the PhC structure is a candidate for a narrow stripe width of less than 1 μm.

IV. Design Considerations of LCI-Membrane-DFB Lasers for On-Chip Optical Interconnects

As discussed in the previous sections, the LCI membrane structure is very attractive for low threshold current operation with high-speed direct modulation capability. Moreover, by introducing a high-index-coupling grating structure such as a surface grating into the LCI membrane structure with a thin core layer, a DFB laser with an extremely low threshold current operation can be expected. In this section, the threshold current and light output power of the LCI-membrane-DFB laser at a fixed bias current are discussed in terms of a high-speed light source for on-chip optical interconnects.

We proposed membrane photonic integrated circuits (PICs) consisting of an LCI-membrane-DFB, an InP-based wire waveguide, and other semiconductor components as shown in Fig. 11 as a candidate for an in-plane photonic platform with extremely low-power consumption [33]. As previously mentioned, the available consumption energy (energy cost for data transport) for a semiconductor laser in an on-chip optical interconnect is estimated to be about 100 fJ/bit or less [6]. This means that the available injection current of the semiconductor light source is limited to less than 1 mA when a data rate of 10 Gb/s and a driving voltage of 1 V are assumed. Therefore, ultralow threshold current and high-speed operations are strongly required. The required output power of the light source is determined from the minimum receivable power of the detector and other losses. We assumed the minimum receivable power of –13 dBm (0.05 mW) which is usually used for a GaInAs p–i–n photodiode (PIN-PD) at a 10-Gb/s transmission rate with a level bit-error rate (BER) of 10^{-9}. Other losses are assumed to be 5 dB in total, as listed in Table I, and hence, the required output power of the light source is estimated to be −8 dBm (0.16 mW) for a 10-Gb/s transmission.

First, we calculated the minimum threshold current for a given index-coupling coefficient κ of an LCI-membrane-DFB laser with a surface grating structure by varying the cavity length, and plotted it as a function of the volume of the active region in Fig. 12, where a stripe width is of 1 μm and a core layer

TABLE I
Device Parameters of a Membrane Based PIC

Minimum receivable power of PIN-PD	0.05 mW (–13 dBm)
Coupling loss between waveguide and PIN-PD	–1.5 dB
Transmission loss in membrane waveguide (2 cm)	–2.0 dB
Coupling loss between waveguide and LD	–1.5 dB
Required output power of LD	0.16 mW (–8 dBm)

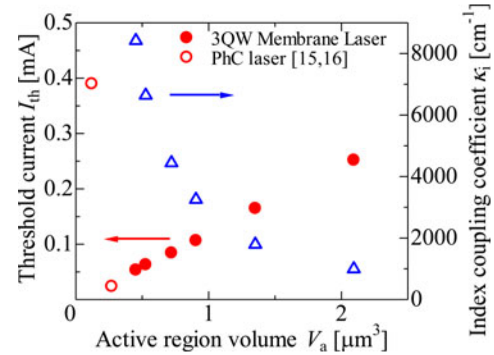

Fig. 12. Calculated threshold current dependence on active region volume of an LCI-membrane-DFB laser.

thickness is of 150 nm. The threshold current was calculated from [34]

$$I_{\rm th} = \frac{eV_aB_{\rm eff}}{\eta_i}\cdot\left(N_g + \frac{1}{\xi(dg/dN)}(\alpha_m + \alpha_{\rm WG})\right)^2 \quad (2)$$

where e is the electron charge, V_a is the active region volume, $B_{\rm eff}$ is the effective recombination coefficient, η_i is internal quantum efficiency, N_g is the transparency carrier density, ξ is the optical confinement factor, dg/dN is the differential gain, $\alpha_{\rm WG}$ is the waveguide loss, and α_m is the mirror loss. Threshold currents of the PhC lasers are also plotted in this figure for comparison [15], [16]. The number of QW was set to be 3 for comparison with that of these PhC lasers. The index-coupling coefficient κ of the membrane laser with the surface grating was calculated by assuming rectangular-shaped grooves with a width of a half period of the grating. As can be seen, an ultralow threshold current in the membrane laser can be achieved by adopting a cavity with a high-index-coupling coefficient and a small active region volume. A threshold current of around 53 μA can be obtained for a cavity length of 25 μm with a 3QW active region and a grating depth of 150 nm (which corresponds to an index-coupling coefficient of 8400 cm^{-1}) is used.

Next, the design of the membrane laser was optimized toward the light source for on-chip optical interconnection. The lasing characteristics of the membrane laser were calculated by using the coupled wave theory [35]. A calculated structure of the LCI-membrane laser with surface grating structure is shown in Fig. 13. As previously reported, the surface grating structure is suitable for LCI-type laser because the surface grating structure can be formed by a simple fabrication process [27], [28]. In addition, the number of QWs was set to be 5 since a larger number

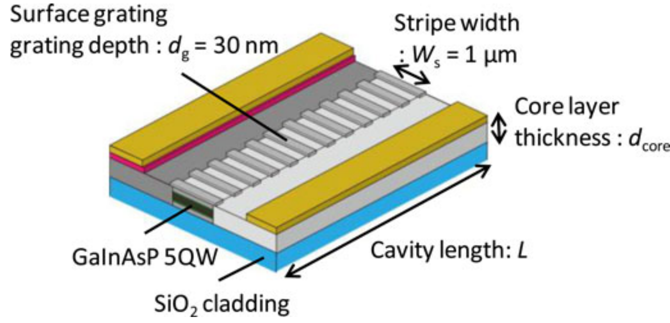

Fig. 13. Calculated structure of an LCI-membrane laser with a surface grating structure.

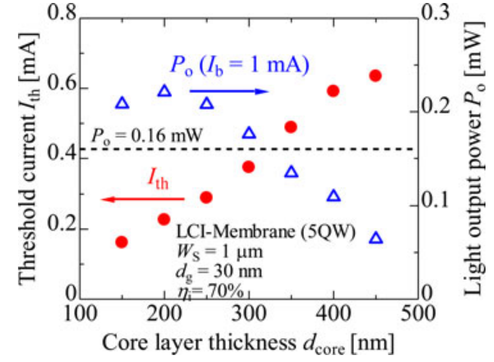

Fig. 14. Calculated threshold current and light output power dependence of core layer thickness of an LCI-membrane-DFB laser.

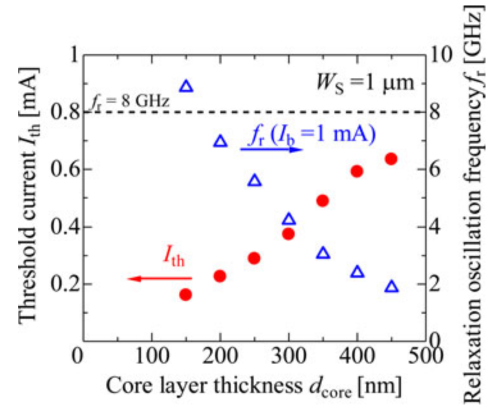

Fig. 15. Calculated threshold current and the relaxation oscillation frequency dependence on core layer thickness of an LCI-membrane-DFB laser.

of QWs has an advantage in maximum light output power and high relaxation oscillation frequency. Therefore, the QW should be multilayered while maintaining a high optical confinement factor and a high coupling coefficient. However, as the number of QWs increases, it becomes difficult to maintain the optical confinement factor and coupling coefficient due to the increase of the total core layer thickness. The maximum number of QWs that could fit into the core layer with a total thickness of less than 150 nm is 5. Furthermore, a surface grating depth and stripe width were also fixed to be 30 nm and 1 μm, respectively. Under this condition, the estimated coupling coefficient is 2900 cm^{-1} when the core layer thickness is 150 nm.

In previous work, the series resistance of the LCI laser on SI–InP was estimated to be about 25 Ω with the core layer thickness of 400 nm and the cavity length of 300 μm [27]. The sheet resistance of this p-InP region was experimentally estimated to be about 2.7 kΩ/□. Because this value is more than 100 times larger than that of n-InP region, the series resistance of the p-InP region mainly causes the high series resistance of the device. In the LCI-type laser, the distance between the edge of the active region and metal electrode in a p-doped region was set to be about 3 μm. By reducing the distance to be 1 μm, the series resistance of the membrane laser is expected to be about 170 Ω even for a short cavity length of 40 μm and a thin core layer thickness of 150 nm, and the driving voltage can be 1 V at a driving current of 1 mA. Actually, microcavity lasers such as VCSELs or PhC lasers also have quite high electrical resistance compared with that of typical semiconductor laser [7], [15], [16]. However, high-speed modulations with ultralow pulse energy of these devices were demonstrated by the reduction of the driving current. Therefore, it is most essential to realize strong optical confinement and small cavity volume from the view point of low energy cost for data transport.

The threshold current and light output power at a bias current of 1 mA of an LCI-membrane-DFB laser as a function of core layer thickness were calculated as shown in Fig. 14. In this calculation, the cavity length of each point was set to be the length which minimized the threshold current. The internal quantum efficiency η_i and differential gain dg/dN were assumed to be 70% and 6.0 × 10^{-16} cm^{-3}, respectively. The threshold current of an LCI-membrane-DFB laser with a core layer thickness of 150 nm was calculated to be 0.16 mA with a cavity length of 40 μm. As previously mentioned, the required light output power of 0.16 mW at an injection current of 1 mA can be obtained with a core layer thickness of less than 300 nm, and the light output power reaches a maximum value of 0.23 mW for a core layer thickness of 200 nm. In the case of the membrane laser with a core layer thickness of 150 nm and a cavity length of 40 μm, the power dissipation due to joule heat generation by an injection current of 1 mA was estimated to be 0.17 mW with assumption of the series resistance of 170 Ω. When the threshold current is reduced to be less than 0.16 mA by reduction of active region volume, the power dissipation due to joule heat generation will increase due to an increase of series resistance. Therefore, the total power dissipation toward enough light output power will also increases with increase of series resistance when the differential quantum efficiency is assumed to be constant. In order to realize the light source with low power consumption, the power dissipation due to joule heat generation should be sufficiently small compared with the total power dissipation.

Fig. 15 shows the threshold current (the same as in Fig. 14) and the relaxation oscillation frequency f_r of an LCI-membrane-DFB laser as a function of core layer thickness at a bias current of 1 mA. The relaxation oscillation frequency can be calculated from

$$f_r = \frac{1}{2\pi\sqrt{\tau_s \tau_p}} \sqrt{\frac{N_{\rm th}}{N_{\rm th} - N_g}} \sqrt{\frac{I_b}{I_{\rm th}} - 1} \quad (3)$$

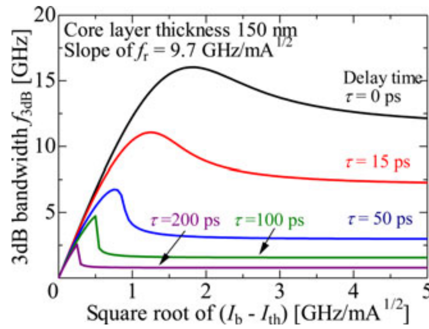

Fig. 16. Calculated 3-dB bandwidth of the LCI- membrane-DFB laser with various delay times.

where τ_s is the carrier lifetime, τ_p is the photon lifetime, N_g is the transparent carrier density, and $N_{\rm th}$ is threshold carrier density. As the core layer becomes thinner, the relaxation oscillation frequency is dramatically enhanced because of an increase in the bias current level (I_b/ $\rm I_{th}$ $-$ 1) as well as that of the optical confinement factor. The relaxation oscillation frequency f_r of 8.9 GHz (at $I_b = 1$ mA) and the modulation current efficiency MCEF of 9.7 GHz/mA$^{1/2}$ were obtained with a core layer thickness of 150 nm. The relaxation oscillation frequency meets the requirements for a light source for 10-Gb/s on-chip optical interconnections. In addition, this MCEF is much higher than conventional long-wavelength LDs. The calculated 3-dB bandwidth of the LCI-membrane-DFB laser, which includes the effect of the delay time, is shown in Fig 16. When the stripe width is 1 μm, the delay time due to the carrier transport in OCLs was estimated to be 15 ps as shown in Fig. 6. The 3-dB bandwidth could be increased to higher than 10 GHz when the delay time is reduced to 15 ps by adopting a narrow stripe width of 1 μm. This result indicates that an LCI-membrane-DFB laser can achieve sufficient practical performance. It was found that the membrane laser can totally meet the requirements for on-chip optical interconnection by optimizing the device structure.

V. Conclusion

In conclusion, we investigated the lasing characteristics of the LCI-membrane-DFB laser for on-chip optical interconnection. First, the stripe width dependence of an LCI-type laser fabricated on SI–InP substrate was measured. As a result, it was found that a narrow stripe width is required for high internal quantum efficiency and small carrier injection delay time. Furthermore, the carrier injection delay time of an LCI laser with a stripe width of 1 μm was estimated to be 15 ps from small-signal analysis of the LCI-FP lasers. This was thought to be sufficient to achieve high-speed modulation of more than 10 Gb/s. Second, the strong optical confinement effect of the membrane laser was theoretically investigated. By reduction of the core layer thickness, the optical confinement factor could be enhanced to about 3.7%/well. Finally, the design of an LCI-membrane DFB laser for on-chip optical interconnection was investigated. It was shown that the light output level and the modulation bandwidth required for 10 Gb/s transmission can be achieved at a bias current of 1 mA by adopting a core layer thickness and stripe width of 150 nm and 1 μm, respectively. From these results, the membrane laser is expected to meet the requirements for on-chip optical interconnection.

Acknowledgment

The authors would like to thank Prof. M. Asada, Prof. F. Koyama, Prof. T. Mizumoto, Prof. Y. Miyamoto, Prof. M. Watanabe, and Dr. Tadashi Okumura, Tokyo Institute of Technology, for fruitful discussions.

References

[1] P. Kapur, J. P. McVittie, and K. C. Saraswat, "Technology and reliability constrained future copper interconnects: Part I. Resistance modeling," *IEEE Trans. Electron. Devices*, vol. 49, no. 4, pp. 590–597, Apr. 2002.

[2] P. Kapur, G. Chandra, J. P. McVittie, and K. C. Saraswat, "Technology and reliability constrained future copper interconnects: Part II. Performance implications," *IEEE Trans. Electron. Devices*, vol. 49, no. 4, pp. 598–604, Apr. 2002.

[3] D. A. B. Miller, "Rationale and challenges for optical interconnects to electronic chips," *Proc. IEEE*, vol. 88, no. 6, pp. 728–749, Jun. 2000.

[4] G. Chen, H. Chen, M. Haurylau, N. A. Nelson, D. H. Albonesi, P. M. Fauchet, and E. G. Friedman, "Prediction of CMOS compatible on-chip optical interconnect," *Integr., VLSI J.*, vol. 40, no. 4, pp. 434–446, Oct. 2006.

[5] K. Ohashi, K. Nishi, T. Shimizu, M. Nakada, J. Fujikata, J. Ushida, S. Torii, K. Nose, M. Mizuno, H. Yukawa, M. Kinoshita, N. Suzuki, A. Gomyo, T. Ishi, D. Okamoto, K. Furue, T. Ueno, T. Tsuchizawa, T. Watanabe, K. Yamada, S. Itabashi, and J. Akedo, "On-chip optical interconnect," *Proc. IEEE*, vol. 97, no. 7, pp. 1186–1198, Jul. 2009.

[6] D. A. B. Miller, "Device requirements of optical interconnects to silicon chips," *Proc IEEE*, vol. 97, no. 7, pp. 1166–1185, Jul. 2009.

[7] P. Moser, W. Hofmann, P. Wolf, J. A. Lott, G. Larisch, A. Payusov, N. N. Ledentsov, and D. Bimberg, "81 fJ/bit energy-to-data ratio of 850 nm vertical-cavity surface emitting lasers for optical interconnects," *Appl. Phys. Lett*, vol. 98, no. 23, pp. 231106-1–231106-3, Jun. 2011.

[8] S. Imai, K. Takaki, S. Kamiya, H. Shimizu, J. Yoshida, Y. Kawakita, T. Takagi, K. Hiraiwa, H. Shimizu, T. Suzuki, N. Iwai, T. Ishikawa, N. Tsukiji, and A. Kasukawa, "Recorded low power dissipation in highly reliable 1060-nm VCSELs for "Green" optical interconnection," *IEEE J. Sel. Topics Quantum Electron.*, vol. 17, no. 6, pp. 1614–1620, Nov./Dec. 2011.

[9] A. Kasukawa, "VCSEL technology for green optical interconnects," *IEEE Photon. J.*, vol. 4, no. 2, pp. 642–646, Apr. 2012.

[10] M. Fujita, R. Ushigome, and T. Baba, "Continuous wave lasing in GaInAsP microdisk injection laser with threshold current of 40 μA," *Electron. Lett.*, vol. 36, no. 9, pp. 790–791, Apr. 2000.

[11] J. V. Campenhout, P. Rojo-Romeo, P. Regreny, C. Seassal, D. V. Thourhout, S. Verstuyft, L. D. Cioccio, J.-M. Fedeli, C. Lagahe, and R. Beaets, "Electrically pumped InP-based microdisk lasers integrated with nanophotonic silicon-on-insulator waveguide circuit," *Opt. Exp.*, vol. 15, no. 11, pp. 6744–6749, May 2007.

[12] S. Matsuo, A. Shinya, T. Kakitsuka, K. Nozaki, T Segawa, T. Sato, Y. Kawaguchi, and M. Notomi, "High-speed ultracompact buried heterostructure photonic-crystal laser with 13 fj of energy consumed per bit transmitted," *Nat. Photon.*, vol. 4, no. 9, pp. 648–654, Sep. 2010.

[13] S. Matsuo, A. Shinya, C.-H. Chen, K. Nozaki, T. Sato, Y. Kawaguchi, H. Taniyama, and M. Notomi, "20-Gbit/s directly modulated photonic crystal nanocavity laser with ultra-low power consumption," *Opt. Exp.*, vol. 19, no. 3, pp. 2242–2250, Jan. 2011.

[14] B. Ellis, M. A. Mayer, G. Shambat, T. Sarmiento, J. Harris, E. E. Haller, and J. Vučković, "Ultralow-threshold electrically pumped quantum-dot photonic-crystal nanocavity laser," *Nat. Photon.*, vol. 5, no. 5, pp. 297–300, May 2011.

[15] S. Matsuo, K. Takeda, T. Sato, M. Notomi, A. Shinya, K. Nozaki, H. Taniyama, K. Hasebe, and T. Kakitsuka, "Room-Temperature continuous-wave operation of lateral current injection wavelength-scale embedded active-region photonic-crystal laser," *Opt. Exp.*, vol. 20, no. 4, pp. 3773–9780, Feb. 2012.

[16] T. Sato, K. Takeda, A. Shinya, K. Nozaki, H. Taniyama, K. Hasebe, T. Kakitsuka, and S. Matsuo, "Ultra-low threshold current CW operation

of photonic crystal nanocavity laser with InAlAs sacrificial layer," in *Proc. 23rd IEEE Int. Semiconductor Laser Conf.*, San Diego, CA, USA, vol. WC4, Oct. 2012.
[17] T. Okamoto, N. Nunoya, Y. Onoda, T. Yamazaki, S. Tamura, and S. Arai, "Optically pumped membrane BH-DFB lasers for low-threshold and single-mode operation," *IEEE J. Sel. Topics Quantum Electron.*, vol. 9, no. 5, pp. 1361–1366, Sep./Oct. 2003.
[18] S. Sakamoto, H. Naitoh, M. Otake, Y. Nishimoto, S. Tamura, T. Maruyama, N. Nishiyama, and S. Arai, "Strongly index-coupled membrane BH-DFB lasers with surface corrugation grating," *IEEE J. Sel. Topics Quantum Electron.*, vol. 13, no. 5, pp. 1135–1141, Sep./Oct. 2007.
[19] S. Sakamoto, H. Naitoh, M. Ohtake, Y. Nishimoto, T. Maruyama, N. Nishiyama, and S. Arai, "85 °C continuous-wave operation of GaInAsP/InP-membrane buried heterostructure distributed feedback lasers with polymer cladding layer," *Jpn. J. Appl. Phys.*, vol. 46, no. 47, pp. L1155–L1157, Nov. 2007.
[20] S. Arai, N. Nishiyama, T. Maruyama, and T. Okumura, "GaInAsP/InP membrane lasers for optical interconnects," *IEEE J. Sel. Topics Quantum Electron.*, vol. 17, no. 5, Sep./Oct. 2011.
[21] T. Maruyama, T. Okumura, S. Sakamoto, K. Miura, Y. Nishimoto, and S. Arai, "GaInAsP/InP membrane BH-DFB lasers directly bonded on SOI substrate," *Opt. Exp.*, vol. 14, no. 18, pp. 8184–8188, Sep. 2006.
[22] H. Naitoh, S. Sakamoto, M. Ohtake, T. Okumura, T. Maruyama, N. Nishiyama, and S. Arai, "GaInAsP/InP membrane BH-DFB laser with air-bridge structure," *Jpn. J. Appl. Phys.*, vol. 46, no. 47, pp. 1158–1160, Nov. 2007.
[23] K. Oe, Y. Noguchi, and C. Caneau, "GaInAsP lateral current injection lasers on semi-insulating substrates," *IEEE Photon. Technol. Lett.*, vol. 6, no. 4, pp. 479–481, Apr. 1994.
[24] T. Okumura, M. Kurokawa, M. Shirao, D. Kondo, H. Ito, N. Nishiyama, T. Maruyama, and S. Arai, "Lateral current injection GaInAsP/InP laser on semi-insulating substrate for membrane-based photonic circuits," *Opt. Exp.*, vol. 17, no. 15, pp. 12564–12570, Jul. 2009.
[25] T. Okumura, H. Ito, D. Kondo, N. Nishiyama, and S. Arai, "Continuous wave operation of thin film lateral current injection lasers grown on semi-insulating InP," *Jpn. J. Appl. Phys.*, vol. 49, no. 4, pp. 040205-1–040205-3, Apr. 2010.
[26] T. Shindo, T. Okumura, H. Ito, T. Koguchi, D. Takahashi, Y. Atsumi, J. H. Kang, R. Osabe, T. Amemiya, N. Nishiyama, and S. Arai, "GaInAsP/InP lateral-current-injection distributed feedback laser with a-Si surface grating," *Opt. Exp.*, vol. 19, no. 3, pp. 1884–1891, Jan. 2011.
[27] T. Shindo, T. Okumura, H. Ito, T. Koguchi, D. Takahashi, Y. Atsumi, J. H. Kang, R. Osabe, T. Amemiya, N. Nishiyama, and S. Arai, "Lateral-current-injection distributed feedback laser with surface grating structure," *IEEE J. Sel. Topics Quantum Electron.*, vol. 17, no. 5, pp. 1175–1182, Sep./Oct. 2011.
[28] T. Shindo, M. Futami, T. Okumura, R. Osabe, T. Amemiya, N. Nishiyama, and S. Arai, "Lasing operation of lateral-current-injection membrane DFB laser with surface grating," presented at the 16th Opto-Electron. Commun. Conf., Kaohsiung, Taiwan, Jul. 2011.
[29] M. Futami, T. Shindo, K. Doi, T. Amemiya, N. Nishiyama, and S. Arai, "Low-threshold operation of LCI-membrane-DFB lasers with Be-doped GaInAs contact layer," presented at the 24th Int. Conf. Indium Phosphide Related Mater., Santa Barbara, CA, USA, vol. Th-2 C.5, Aug. 2012.
[30] M. Futami, T. Shindo, T. Koguchi, K. Shinno, T. Amemiya, N. Nobuhiko, and S. Arai, "GaInAsP/InP lateral current injection laser with uniformly distributed quantum wells structure," *IEEE Photon. Technol. Lett.*, vol. 24, no. 11, pp. 888–890, Jun. 2012.
[31] M. Futami, K. Shinno, T. Shindo, K. Doi, T. Amemiya, N. Nobuhiko, and S. Arai, "Improved quantum efficiency of GaInAsP/InP top air-clad lateral current injection lasers," presented at the 1st Opt. Interconnects Conf., vol. TuB-3, May 2012.
[32] H. Hirayama, J. Yoshida, Y. Miyake, and M. Asada, "Estimation of carrier capture time of quantum-well lasers by spontaneous emission spectra," *Appl. Phys. Lett.*, vol. 61, no. 20, pp. 2398–2400, Nov. 1992.
[33] J. Lee, Y. Maeda, Y. Atsumi, Y. Takino, N. Nishiyama, and S. Arai, "Low-loss GaInAsP wire waveguide on Si substrate with benzocyclobutene adhesive wafer bonding for membrane photonic circuits," *Jpn. J. Appl. Phys.*, vol. 51, no. 4, pp. 042201-1–042201-5, Mar. 2012.
[34] M. Asada and Y. Suematsu, "The effects of loss and nonradiative recombination "the temperature dependence of threshold current in 1.5–1.6 μm GaInAsP/InP lasers," *IEEE J. Quantum Electron.*, vol. QE-19, no. 6, pp. 917–922, Jun. 1983.
[35] H. Kogelnik and C. V. Shank, "Coupled-wave theory of distributed feedback lasers," *J. Appl. Phys.*, vol. 43, no. 5, pp. 2327–2335, May 1972.

Takahiko Shindo (S'10–M'12) received the B.E., M.E., and Ph.D. degrees in electrical and electronic engineering from the Tokyo Institute of Technology, Meguro-ku, Tokyo, Japan, in 2008, 2010, and 2012, respectively.

He is currently with Quantum Nanoelectronics Research Center (QNERC), Tokyo Institute of Technology. Since 2010, he has also been a Research Fellow at the Japan Society for the Promotion of Science (JSPS), Japan. His current research interests include photonic integrated devices on a silicon platform.

Dr. Shindo is a student member of the Japan Society of Applied Physics.

Mitsuaki Futami was born in Saitama Prefecture, Japan, in 1988. He received the B.E. degree in electrical and electronic engineering from the Tokyo Institute of Technology, Tokyo, Japan, in 2012, where he is currently working toward the M.E. degree in the Department of Electrical and Electronic Engineering.

His current research interests include membrane-based photonic devices for optical interconnection.

Mr. Futami is a member of the Japan Society of Applied Physics.

Kyohei Doi was born in Saitama Prefecture, Japan, in 1988. He received the B.E. degree in electrical and electronic engineering from the Tokyo Institute of Technology, Tokyo, Japan, in 2012, where he is currently working toward the M.E. degree in the Department of Electrical and Electronic Engineering.

His current research interests include membrane-based photonic devices for optical interconnection.

Mr. Doi is a member of the Japan Society of Applied Physics.

Tomohiro Amemiya (S'06–M'09) received the B.S., M.S., and Ph.D. degrees in electronic engineering from the University of Tokyo, Tokyo, Japan, in 2004, 2006, and 2009, respectively.

In 2009, he moved to the Quantum Nanoelectronics Research Center, Tokyo Institute of Technology, where he is currently an Assistant Professor. His research interests are in the physics of semiconductor light-controlling devices, metamaterials for optical frequency, magneto-optical devices, and processing technologies for fabricating these devices.

Dr. Amemiya is a member of the Optical Society of America, the American Physical Society, and the Japan Society of Applied Physics. He received the 2007 IEEE Photonics Society Annual Student Paper award and the 2008 IEEE Photonics Society Graduate Student Fellowship.

Nobuhiko Nishiyama (M'01–SM'07) was born in Yamaguchi Prefecture, Japan, in 1974. He received B.E., M.E., and Ph.D. degrees from the Tokyo Institute of Technology, Tokyo, Japan, in 1997, 1999, and 2001, respectively. During his Ph.D. work, he demonstrated single-mode 0.98- and 1.1-μm VCSEL arrays with stable polarization using misoriented substrates for high-speed optical networks as well as MOCVD-grown GaInNAs VCSELs.

He joined Corning, Inc., NY in 2001 and was with the Semiconductor Technology Research Group. At Corning, Inc., he worked on several subjects including short-wavelength lasers, 1060-nm DFB/DBR lasers, and long-wavelength InP-based VCSELs. Since 2006, he has been an Associate Professor at the Tokyo Institute of Technology. His main research interests include transistor lasers, silicon photonics, III–V silicon hybrid optical devices, and THz-optical signal conversions involving optics-electronics-radio integration circuits.

Dr. Nishiyama received an Excellent Paper Award from the Institute of Electronics, Information and Communication Engineers (IEICE) of Japan in 2001 and the Young Scientists Prize in the Commendation for Science and Technology from the Minister of Education, Culture, Sports, Science and Technology in 2009. He is a member of the Japan Society of Applied Physics, IEICE, and IEEE Photonics Society. He is currently a Chair of the technical group of silicon photonics in IEICE.

Shigehisa Arai (M'83–SM'06–F'10) was born in Kanagawa Prefecture, Japan, in 1953. He received the B.E., M.E., and D.E. degrees in electronics from the Tokyo Institute of Technology, Meguro-ku, Tokyo, Japan, in 1977, 1979, and 1982, respectively. During his Ph.D. work, he demonstrated room-temperature CW operations of 1.11–1.67-μm-long-wavelength lasers fabricated by liquid-phase epitaxy as well as their single-mode operations under rapid direct modulation.

He joined the Department of Physical Electronics, Tokyo Institute of Technology, as a Research Associate in 1982, and joined AT&T Bell Laboratories, Holmdel, NJ, USA, as a Visiting Researcher from 1983 to 1984, on leave from the Tokyo Institute of Technology. He became a Lecturer in 1984, an Associate Professor in 1987, and a Professor with the Research Center for Quantum Effect Electronics and the Department of Electrical and Electronic Engineering in 1994. Since 2004, he has been a Professor with the Quantum Nanoelectronics Research Center, Tokyo Institute of Technology. His research interests include photonic integrated devices such as dynamic-single-mode and wavelength-tunable semiconductor lasers, semiconductor optical amplifiers, and optical switches/modulators. His current research interests include studies of low-damage and cost-effective processing technologies of ultrafine structures for high-performance lasers and photonic integrated circuits on silicon platforms.

Dr. Arai is a member of the Optical Society of America, the Institute of Electronics, Information and Communication Engineers (IEICE), and the Japan Society of Applied Physics (JSAP). He received an Excellent Paper Award from the IEICE of Japan in 1988, the Michael Lunn Memorial Award from the Indium Phosphide and Related Materials Conference in 2000, Prizes for Science and Technology including a Commendation for Science and Technology from the Minister of Education, Culture, Sports, Science and Technology in 2008, an Electronics Society Award and the Achievement Award from IEICE in 2008 and 2011, respectively, and a JSAP Fellowship in 2008.